Electron Acceleration in an Ultraintense-Laser-Illuminated Capillary

Yoneyoshi Kitagawa,[1,*] Yasuhiko Sentoku,[2] Shin Akamatsu,[1] Wataru Sakamoto,[1] Ryosuke Kodama,[1] Kazuo A. Tanaka,[1] Ken Azumi,[1] Takayoshi Norimatsu,[1] Takeshi Matsuoka,[1] Hisanori Fujita,[1] and Hidetsugu Yoshida[1]

[1]*Institute of Laser Engineering, Osaka University, Suita, Osaka 565-0871, Japan*

[2]*Department of Physics, University of Nevada, Reno, 5625 Fox Avenue, Reno, Nevada 89506, USA*

(Received 30 July 2003; published 19 May 2004)

An ultraintense laser injected a 10 J of power at 1.053 μm in 0.5 ps into a glass capillary of 1 cm long and 60 μm in diameter and accelerated plasma electrons to 100 MeV. One- and two-dimensional particle codes describe wakefields with 10 GV/m gradient excited behind the laser pulse, which are guided by a plasma density channel far beyond the Rayleigh range. The blueshift of the laser spectrum supports that a plasma of 10^{16} cm^{-3} is inside the capillary. A bump at the high energy tail suggests the electron trapping in the wakefield.

DOI: 10.1103/PhysRevLett.92.205002 PACS numbers: 52.35.Mw, 41.75.Jv, 52.38.Kd

The laser-plasma accelerator concept [1] has been first demonstrated by two frequency CO_2 laser beats [2,3], which have accelerated electrons up to 22 MeV [2] and are now over 200 MeV [4]. The simplest idea of the laser-plasma accelerator is a laser wakefield [5,6]. If a strong laser pulse "bullet" is injected into a plasma and the plasma wavelength is close to the pulse length, its strong photon pressure or ponderomotive force splashes the plasma electrons out of the pulse. Then in the next half wavelength the electrons return back, making a plasma wave, a space charge wave oscillating at the plasma frequency and propagating behind the laser pulse [7,8]. The electrons, once trapped in the wakefield potential with a retarded phase, are accelerated until they enter the deceleration phase in the potential or the dephasing takes place [5].

Thus far, a gas jet is mainly used for the plasma source, so that the acceleration length is limited to 2 mm or less. This is only a few times larger than the Rayleigh range, written as $z_R = \pi r_0^2/\lambda_0$, where r_0 is a laser spot radius and λ_0 is the laser wavelength. The ultraintense lasers have dramatically increased the acceleration gradient from 1 GV/m of the above-mentioned CO_2 laser beat-wave [2] to hundreds of GV/m of a self-modulated wakefield [9,10] or other schemes [4]. Nevertheless, nothing makes the plasma length longer. The acceleration gain is, therefore, limited to a few 100 MeV level. Suppose the size of a plasma is much longer than z_R and is close to the dephasing limit, $\lambda_p \gamma_\phi^2/\pi$. Here λ_p is the plasma wavelength and the square of a relativistic factor γ_ϕ^2 is a ratio of the cutoff plasma density n_c to the electron density n_e [5]. Then the dephasing limit is typically 30 cm for 10^{17} cm^{-3}. In the relativistic laser regime, the maximum acceleration field is approximated by $E_{\max} \sim E_{wb} a_0 = m\omega_p c a_0/e \sim E_L/\gamma_\phi$, where E_{wb} is the classical wave breaking field $\sim 30\sqrt{n_e/10^{17}\ \mathrm{cm}^{-3}}$ [GV/m], and a_0 the normalized laser field $eE_L/m\omega_0 c$ [11]. If a laser of $a_0 = 2$ transmits 30 cm under a 10^{17} cm^{-3} plasma, electrons obtain a gain of $eE_{\max} \times 30\ \mathrm{cm} > 18$ GeV. Many theoretical and experimental efforts, such as z pinches, axicon channels, and capillaries, are dedicated to make the acceleration length longer [5,12–22].

On the other hand, the maximum energy gain $W_{\max}$, which the electrons obtain within the dephasing limit, is written as $2mc^2\gamma_\phi^2 a_0^2/\sqrt{1 + a_0^2/2}$. So, if you want to have GeV electrons, since a_0 is 1–4 for (2×10^{18})–(2×10^{19}) W cm^{-2}, γ_ϕ must be larger than 15, which means that the electron density must be less than 10^{19} cm^{-3}. Then, we need a thin but cm-class plasma. Some have realized 2–10 cm plasma columns [17,18,22], but no electron acceleration has been yet reported, except for [12]. Injecting a 500 ps 0.4 TW glass laser into a plastic capillary of 150 μm in diameter and 1.58 mm in length had accelerated plasma electrons to >1.4 MeV (the detector limit). Now we report on the 1-cm long capillary acceleration of electrons to 100 MeV.

The acceleration above the wave breaking due to the trapping in the beat wave is reported [23]. The trapping, though in the different parameters, is also discussed in [24]. Here we show an energy bump due to the trapping.

The one-dimensional particle-in-cell simulation (1D-PIC) shows the density dependence of the acceleration gradient, which suggests that the plasma density is around 6×10^{16} in the capillary. The two-dimensional PIC simulation (2D-PIC) demonstrates the pulse guiding in a density channel far beyond the Rayleigh range and explains the electron spectral shape in a process of trapping and radial dephasing. The particle trapping and bunching is an important step to cool the accelerated beams.

The GEKKO-MII CPA laser provided 15 J of power at 1.053 μm in ~0.45–0.7 ps [25,26]. As seen in Fig. 1(a), the laser beam is focused to the capillary edge by an off-axial-parabola mirror of $f/3.8$. 68% of the beam energy is deposited to a 25 μm spot. z_R is 490 μm. The focal intensity I_L is 3×10^{18} W cm^{-2}. The laser is aligned with the capillary axis and 40% of the energy

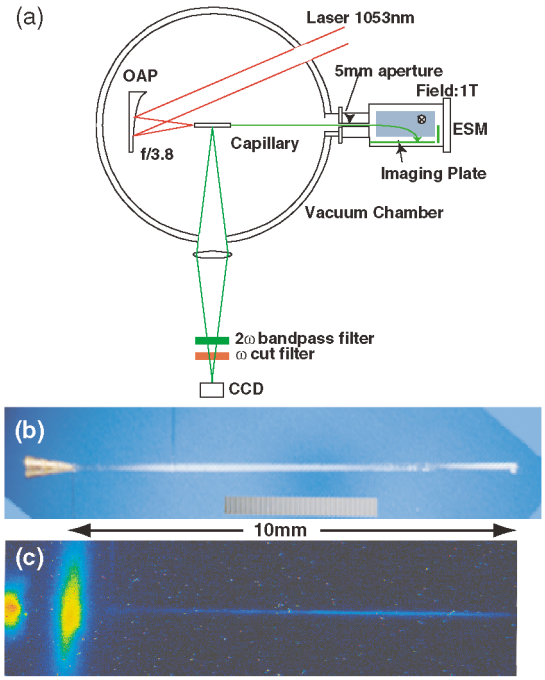

FIG. 1 (color). (a) Experimental setup. (b) Side view of glass capillary. (c) Emission around 527 nm along the capillary axis. Two bright spots at the left-hand side are from the cone entrance and exit, respectively. Horizontal narrow emission is from inside the capillary.

is transmitted through the capillary of 10 mm in length and 60 μm in diameter. The capillary is broken for each shot.

There are two leading prepulses 0.7 and 6.3 ns prior to the main pulse, respectively, with an intensity ratio of $1–3 \times 10^{-3}$ to the main pulse. A probe laser interferometry has shown that the prepulses ablate a plane target surface to generate plasmas when the main pulse comes there, which suggests a low density plasma inside the capillary due to the prepulses. We tried to change the capillary plasma density by changing its inner diameter (bore size).

Figure 1(b) shows the 10-mm long capillary with a guiding cone. The bore size D is 60 μm. The wall thickness is typically 60 μm. To guide the laser light into the capillary, a gold cone is glued to the entrance of the capillary. The cone is 1 mm in length and 0.5 mm in aperture at the entrance and 60–30 μm at the exit, which is fit to the capillary size. The cone angle is 30°, which is twice the laser focusing angle.

The side view of the $2\omega_0$ emission at 527 nm is imaged on a charge coupled device camera through a 5 nm wavelength window. Figure 1(c) is the side image of the laser produced plasma inside the capillary on the same scale as 1(b). The diameter of the emission column was 80 μm in a full width at half maximum, and agrees with the bore size, considering the refractive index of the capillary wall as well as the telescope resolution of 10 μm. Without the guiding cone, the intense laser beam could not be focused into the capillary of 100 μm or less in the bore size. Since no gas is filled, the pressure in the capillary is at a level of the background $\sim 10^{-5}$ Torr.

An electron spectrometer (ESM) is set 1.2 m apart on the capillary axis, consisting of a one-Tesla permanent dipole magnet (NEOMAX) and an imaging plate (IP) (Fuji BAS-SR2025). At the entrance is a 5-mm aperture and 50-mm long acrylic resin piece, followed by a similar stainless steel piece, collimating the electrons ($f/240$). The aperture size limits the energy resolution to 2 MeV. The IP is covered with a 5 μm thick aluminum film. The collection solid angle is 1.36×10^{-5} sr. Using both 10–30 MeV L-band and 30–100 MeV S-band linacs, we have calibrated the spectral sensitivity of IP [27]. The sensitivity to the electron decreases when increasing the beam energy up to 11.5 MeV, then is almost flat to the value of 0.007 PSL/electron $\pm 10\%$ up to 100 MeV. PSL is a relative IP unit named after the photostimulated luminescence.

Figure 2(a) shows that a 10-mm long capillary has a 10 times higher gain than the 1.2-mm long one for the same 60 μm bore. Furthermore, the 10-mm capillary shows a big shoulder at 20 MeV and a small bump at 60 MeV slowing down to the maximum at 100 MeV. The slope temperature is 3 MeV. Charge of the electrons, integrated from 4 to 7 MeV and emitted into the same angle as the laser focal cone (0.054 sr), is estimated as 13 nC. The 1.2-mm capillary shows a small 4.5 MeV shoulder [a dark blue line in 2(a)]. The maximum is only 10–12 MeV and no clear bump is shown. The slope temperature is 0.65 MeV. The spectrum is not much different from just a cone (no capillary is glued).

The capillary length is varied from 0 to 20 mm and D from 30 to 120 μm, respectively. Thus far, a 10 mm length provides the highest gain under the present experimental conditions.

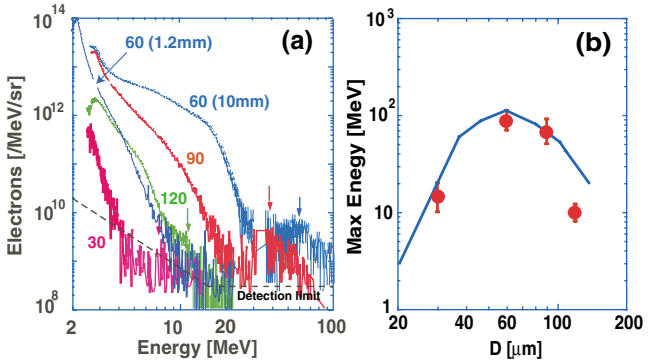

FIG. 2 (color). (a) Electron spectrum for various D at 10 mm long: 30 μm (laser: 7 J); 60 μm (9.2 J); 90 μm (9.2 J); 120 μm (9.2 J); as well as 60 μm (7.3 J) at 1.2 mm long. Arrows indicate bumps. (b) Comparison of maximum energy between experiment (dots) from (a) and 1D-PIC (solid line). Error bar is the reading one.

The maximum energy of 100 MeV for 10 mm suggests that the averaged acceleration field is $\sim$10 GV/m. The plasma density resonant to the pulse length of 0.5 ps is 6×10^{16} cm^{-3} [6], which gives $\sim E_{wb}$–21 GV/m.

As in Fig. 2(a), increasing D from 60 to 120 μm decreases the maximum energy from 100 to 12 MeV and the bump from 70 to 8 MeV, respectively. Decreasing D to 30 μm also decreases the maximum energy to 20 MeV and the bump to 12 MeV. The results show that the 60 μm bore is optimum to accelerate electrons. This may be due to the fact that increasing D decreases the laser intensity I_L and n_e in the capillary; too small bore will make the plasma density too high to excite the wakefield. From 2(a), we plotted the maximum energy in 2(b) as well as the 1D-PIC curve for the 10-mm long capillary using a fixed pulse condition, 0.5 ps and $a_0 = 2$ [28]. The 1D-PIC gives a peak gain of 110 MeV at 6×10^{16} cm^{-3} after 10 mm acceleration. The gain decreases to 40 MeV ($1/e$) as either increasing n_e to 5×10^{17} cm^{-3} or decreasing it to 10^{16}. So, assuming that $n_e \propto D^{-2}$ and $E_L \propto D^{-1}$, we have plotted the density variation of the 1D-PIC peak gain as a function of D, where we fit 6×10^{16} cm^{-3} to $D = 60$ μm. The curve well agrees with the experiments except for 120 μm. In the case of $D = 120$ μm, the measured maximum energy is smaller than the prediction by 1D-PIC. It may be due to the multidimensional effects such as an off-centered staggering propagation.

As the propagation distance is changed from 2 to 10 mm, the 1D-PIC describes that the electrons, trapped in the fixed phases of the wakefield as in Fig. 3(a), grow as in 3(b). Thus, the maximum energy is increased from 10 to 100 MeV as in 3(c). The spectral bumps at the maximum edge in 3(c) agree with the experiments in Fig. 2(a), suggesting the electron trapping in the wakefield. The energy gain is roughly proportional to the transmission distance. For both the 2 and the 10 mm cases, the acceleration field is 10 GV/m, which agrees with the experiment. Though the 1D modeling does not include the optical pulse diffraction, this agreement suggests that the pulse is guided in the capillary without diffraction and the experiment is close to the one-dimensional situation, even if the spot size is less than the plasma wavelength, which is discussed in Ref. [11].

The 2D-PIC describes the laser pulse propagation in the capillary. The radial profile of the plasma density is modeled as a 1×10^{18} cm^{-3} flat bottom is surrounded by a parabolic wall up to 2×10^{19} cm^{-3}. The plasma length is 1.4 mm. The longitudinal profile of the laser pulse is a Gaussian. The pulse length and intensity are 66 fs and 5×10^{18} W cm^{-2}, respectively. The transverse profile is also the Gaussian and its full width at half maximum is 20 μm. z_R is about 314 μm. The laser is injected in parallel at $X = 0$ mm. The total simulation time is 4.6 ps and the simulation box is 1.4 mm $\times$ 51 μm. The simulation is performed on NEC SX4 using 16 CPU with 20 GB memory. Although these simulation parameters are different from the experiments due to the machine capacity, the simulation has enough capability to see the pulse guiding and electron acceleration including trapping and electron acceleration in the capillary.

The laser pulse propagates keeping its intensity over 4 times z_R. The pulse envelope is slightly oscillating with a $2z_R$ period and is guided in the small density gap $\Delta n_e \sim 1 \times 10^{18}$ cm^{-3}, which is close to the analytical estimation given by $\Delta n_e = 1/\pi r_e r_0^2$, where r_e is the classical electron radius in [11].

In Fig. 4(a), the axial phase space of electrons shows not only the discrete trapped electron peaks but also the continuous dephased electrons at $\sim$2–4 MeV, which are not observed in the 1D-PIC results in Figs. 3(a) and 3(b). The 2D-PIC shows that the longitudinal and transverse wakefields are excited simultaneously. The transverse electric fields (E fields) push out the off-centered

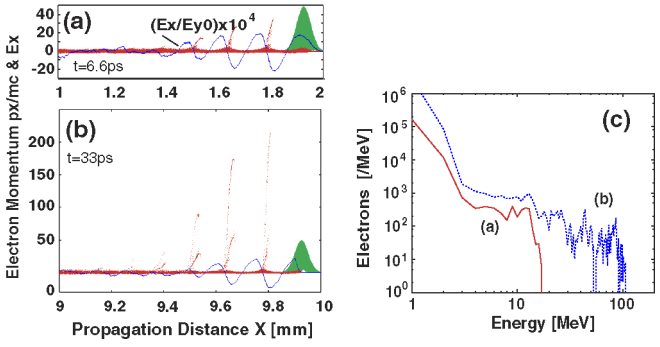

FIG. 3 (color online). 1D-PIC results for $n_e = 6 \times 10^{16}$ cm^{-3}. Electrons are trapped in a fixed phase of the wakefield, generated by the right-going laser pulse (a) at 2 mm or 6.6 ps, (b) at 10 mm or 33 ps. (c) Resulting spectra show bumps at the maximum edge.

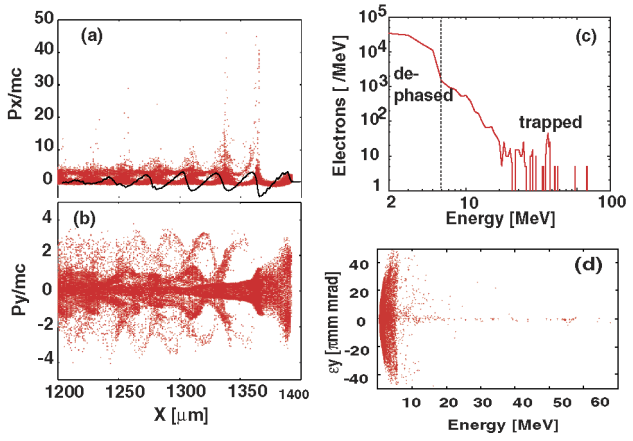

FIG. 4 (color online). 2D-PIC of the laser pulse propagation and electron acceleration in the capillary plasma. (a) Electron axial and (b) transverse phase spaces. (c) Electron energy spectrum at 4.6 ps (after the pulse propagates 1.4 mm). (d) Electron transverse emittance as a function of energy.

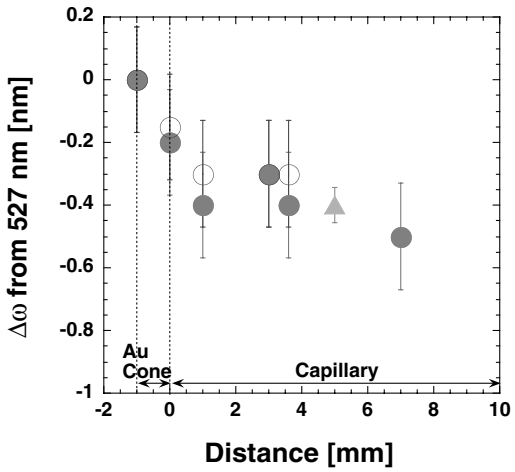

FIG. 5. Blueshift of the second harmonics as a function of the distance from the entrance of the capillary: 60 μm bore and 10 mm long. Different marks correspond to different shots. The fitted curve gives $n_e = (6.2 \pm 0.5) \times 10^{16}$ cm^{-3}.

electrons from the acceleration phase, as seen in the transverse phase space in 4(b). Thus, only the electrons placed at the central region can be trapped in a long distance. The resulting spectrum is in 4(c). We can see the trapped particles bump around the maximum, here around 50 MeV, and the shoulder at the middle energy, here 10 MeV, both of which are in the acceleration phase in the potential well. We also see the low energy plateau from the radial dephasing around a few MeV. These three features amazingly agree with the experimental spectrum, as seen in Fig. 2(a). From Figs. 4(a) and 4(b), we estimated the transverse divergence P_y/P_x (energy spread) to be 2.8×10^{-3} at 15 MeV. The normalized emittance $\epsilon_y = \beta_x \gamma_x \sigma P_y/P_x$ is plotted as a function of energy in 4(d). $\epsilon_y \sim 5\pi$ mm mrad (HWHM) from 15 to 140 MeV.

Figure 5 shows the blueshift of the transmitted light, which suggests the thin plasma formation in the capillary. If the shift is due to the ionization, we can estimate the plasma density increment from the slope [29]. The slope of the blueshift of the second harmonics against the distance $\Delta n/\Delta l = 0.055 \pm 0.005$ nm/mm provides $n_e = (6.2 \pm 0.5) \times 10^{16}$ cm^{-3}, also in agreement with the PIC prediction. The other mechanism would be possible, such as the direct laser acceleration [30], but the plasma density is not so high as the direct laser acceleration effectively occurs.

We have detected the electrons from the pure cone, but the energy was below 10 MeV, which seems to be due to the laser-wall interaction and lower than the detected few tens MeV.

A 7–10 J-1.053 μm pulse in 0.5 ps was injected into a glass capillary of 1 cm in length and 60 μm in bore size, which accelerated plasma electrons to 100 MeV via the laser wakefield inside the capillary. The plasma length is longer than that of any gas jet plasmas. A small energy peak (a bump) is observed at 60 MeV, suggesting the electron trapping in the wakefield. The 1D- and 2D-PICs support the trapping effects both at the middle energy shoulder and at the high energy bump around maximum. The gain dependence on the bore size shows the resonance feature of the laser wakefield. The capillary confines the laser pulse as well as the plasma over a distance much longer than the Rayleigh range.

*Electronic address: yoneyosi@ile.osaka-u.ac.jp

[1] T. Tajima and J. M. Dawson, Phys. Rev. Lett. **43**, 267 (1979).
[2] Y. Kitagawa *et al.*, Phys. Rev. Lett. **68**, 48 (1992).
[3] C. E. Clayton *et al.*, Phys. Rev. Lett. **70**, 37 (1993).
[4] V. Malka *et al.*, Science **298**, 1596 (2002).
[5] T. Tajima, Laser Part. Beams **3**, 351 (1985).
[6] P. Sprangle *et al.*, Comments Plasma Phys. Controlled Fusion **12**, 191 (1989).
[7] J. R. Marquès *et al.*, Phys. Rev. Lett. **76**, 3566 (1996).
[8] C. W. Siders *et al.*, Phys. Rev. Lett. **76**, 3570 (1996).
[9] Y. Kitagawa *et al.*, in *Advanced Accelerator Concepts, Tenth Workshop Mandalay Beach, California, 2002*, edited by C. Clayton and P. Muggi, AIP Conf. Proc. No. 647 (AIP, New York, 2002), p. 634.
[10] A. Modena *et al.*, Nature (London) **377**, 606 (1994).
[11] P. Sprangle, E. Esarey, and A. Ting, Phys. Rev. A **41**, 4463 (1990).
[12] H. Shiraga *et al.*, Meeting Abstracts Phys. Soc. Japan, Vol. 49, Issue 2, Pt. 2, 3aF12 (1984), in Japanese.
[13] S. Jackel *et al.*, Opt. Lett. **20**, 1086 (1995).
[14] G. Shvets *et al.*, IEEE Trans. Plasma Sci. **24**, 351 (1996).
[15] Y. Ehrlich *et al.*, Phys. Rev. Lett. **77**, 4186 (1996).
[16] F. Dorchies *et al.*, Phys. Rev. Lett. **82**, 4655 (1999).
[17] D. Kaganovich *et al.*, Phys. Rev. E **59**, R4769 (1999).
[18] T. Hosokai *et al.*, Opt. Lett. **25**, 10 (2000).
[19] M. C. Downer *et al.*, in *Advanced Accelerator Concepts, Tenth Workshop Mandalay Beach, California, 2002* (Ref. [9], p. 654).
[20] D. J. Spence and S. M. Hooker, Phys. Rev. E **63**, R015401 (2000).
[21] C. Courtois *et al.*, Phys. Plasmas **8**, 3445 (2001).
[22] A. Butler, D. J. Spence, and S. M. Hooker, Phys. Rev. Lett. **89**, 185003 (2002).
[23] M. Everett *et al.*, Nature (London) **368**, 527 (1994).
[24] A. Pukov and J. Meyer-ter-Vehn, Appl. Phys. B **74**, 355 (2002).
[25] M. Mori *et al.*, Nucl. Instrum. Methods Phys. Res., Sect. A **410**, 367 (1998).
[26] Y. Murakami *et al.*, Phys. Plasmas **8**, 4138 (2001).
[27] T. Takahashi *et al.*, Ionizing Radiation **28**, 203 (2002), in Japanese.
[28] Y. Sentoku *et al.*, Phys. Plasmas **5**, 4366 (1998).
[29] E. Yablonovitch, Phys. Rev. Lett. **60**, 795 (1988).
[30] A. Pukov *et al.*, Phys. Plasmas **6**, 2847 (1999).